Chapter 9
Using X-ray Radiography to Observe Fe Distributions in Bioturbated Sediment

Murray K. Gingras, John-Paul Zonneveld and Kurt O. Konhauser

Contents

Abstract The presence of an active iron cycle in modern intertidal sediment from Willapa Bay is confirmed using X-ray radiography and X-ray diffraction (XRD) analyses. The data show that Fe minerals are present in two different redox states. The first is maghemite (Fe_2O_3), which formed on the linings of irrigated burrows. The second is pyrite (FeS_2), which formed as haloes around abandoned or filled burrows. Some pyrite halos coalesced to form nodules of pyrite around the burrow fabric. The mineral paragenesis occurred as follows: (a) detrital ferrous-rich sediment (e.g., pyroxene or organometallic complexes) is buried and progressively dissolved to Fe^{2+}; (b) the Fe^{2+} either reacts with pore-water sulfide (formed via bacterial sulfate reduction) to form pyrite in the matrix or it diffuses to the burrow margins where it is oxidized to form maghemite; (c) when the burrows become abandoned and isolated from the overlying oxic seawater, the ferric iron is biologically reduced to Fe^{2+} (via bacterial iron reduction) where it repeats Step 2. The pyrite

M. K. Gingras (✉) · J.-P. Zonneveld · K. O. Konhauser
Department of Earth and Atmospheric Science, University of Alberta, 1-26 Earth Science Building, Edmonton, Alberta, T6G 2E3, Canada
e-mail: mgingras@ualberta.ca

D. I. Hembree et al. (eds.), *Experimental Approaches to Understanding Fossil Organisms,* Topics in Geobiology 41, DOI 10.1007/978-94-017-8721-5_9,

remains stable unless exposed again to oxidizing conditions, such as later bioturbation. The inchoate nodules appear to form in less than a decade. Interestingly, the mineral distributions observed here are reminiscent of nodules observed in several other marginal marine settings, particularly those that have an oxidized-Fe-mineral core and a pyrite rind. Although those nodules are normally taken to infer evolving pore-water compositions, perhaps they are more simply explained by the processes reported above.

Keywords Fe Nodule · Early diagenesis · Invertebrate burrows · Burrow-Facilitated cementation

9.1 Introduction

In marine settings, burrows are important loci for the precipitation and concentration of seawater-, pore water-, and sediment-derived cations. This is a result of burrows being enriched in organics, such as extra polymeric substances (EPS) in the burrow margins, and associated fecal material (see Konhauser and Gingras 2007 for a summary). These locally concentrated organics promote steep geochemical gradients from the oxygenated burrow into adjacent suboxic sediment (Aller 1980; Aller et al. 1998; Zorn et al. 2006). In instances where the burrow is active, and thus irrigated by its tenant, the burrow wall is exposed to oxidizing conditions and, in most cases, the redox conditions sharply grade to reducing conditions in the sediment. As a result, cations, including those of Fe and Mn, can be enriched on the burrow lining, but when the burrow is abandoned and becomes suboxic, those metal cations can become remobilized.

The accumulation and redistribution of cations in bioturbated sediments is important to later diagenetic processes, such as the precipitation of dolomite, ferroan cements, and in the development of nodules, as commonly the source of Fe or Mg in those processes is unknown. This chapter attempts to use X-ray radiography of modern bioturbated sediment to observe some of the ways that Fe is stored and redistributed in association with biogenic sedimentary structures. The aim is to characterize the different phases of Fe mineralization observed in, and near, the burrows to estimate the rate of Fe diffusion into the sediment, and to visualize the cycling of Fe in an example of intertidal sediment.

9.2 Background

Although the observation of metal enrichment in burrow-associated cements is routine, only a few studies have attempted to quantify the amount of metal enrichment associated with burrow-margin cementation. In one of the first quantitative studies of metal enrichment in burrow linings, Over (1990) observed that Fe, Mn, Cu, Ni, and Zn were preferentially concentrated within modern and Holocene burrow

linings. Metal enrichment occurred as oxide or oxyhydroxide coatings under oxic conditions, as sulfide or phosphate phases under reducing conditions, or as organometallic complexes. Several other studies associate Fe enrichment in burrows to a range of processes. Carpenter et al. (1988) showed that nodule formation in the Cretaceous Fox Hills Formation (North Dakota) resulted from incipient glaucony associated with fecal material in bioturbated media. The post-depositional pyrite-cementation of worm burrows was examined by Virtasalo et al. (2012). Zorn et al. (2006) established a paragenetic model of Fe-rich nodule formation associated with *Rosselia* in Cretaceous (Horseshoe Canyon Formation) strata from Alberta. Iron has even been shown to be stored in burrows through passive infilling with goethite spherules (Rodriguez-Tovar 2005). Enrichment of metal ions has also been considered as a mechanism to explain burrow-associated dolomite in carbonate-bearing units (Gingras et al. 2004; Rameil 2008; Corlett and Jones 2012).

Less work has been conducted on the relationship between modern burrows and their role in Fe cycling in modern sediments. Löwemark and Schäfer (2003) reported the association of pyrite framboids in recent sediments that contained waste-stowage burrows. Another example of a modern biology Fe association was provided by Ferreira et al. (2007). In a study of mangrove root- and crab burrow-associated Fe, it was shown that pyrite was more abundant in more heavily vegetated zones (Ferreira et al. 2007). Thus, it appears that more oxidizing conditions and pyrite oxidation processes promote iron oxyhydroxide precipitation (Ferreira et al. 2007). Moreover, several workers have reported the general association of Fe and bioturbation in some modern sediments (Gingras et al. 1999; Wetzel 2008), but these reports do not focus on the characterization of the Fe phase.

9.3 Study Area

All of the discussed samples come from the Palix River in the brackish and tidal zone of Willapa Bay, Washington, USA (Fig. 9.1). The samples are from the box cores taken at the lower intertidal flat adjacent to the fluvio-tidal channels. Locations of the slab images presented in Fig. 9.2 are indicated in Fig. 9.1. The sedimentology and ichnology of Willapa Bay are well studied and are summarized in Clifton (1983) and Gingras et al. (1999). Bynum (2007) showed that the river-derived sediments are clinopyroxene rich and are from the Willapa Highlands immediately east of Willapa Bay.

9.4 Material and Methods

All of the samples were collected in July, 2011. One of the samples contains a lead-shot marker bed placed in 2010 to indicate the seasonal sedimentation rate and provide a time line in the sediment.

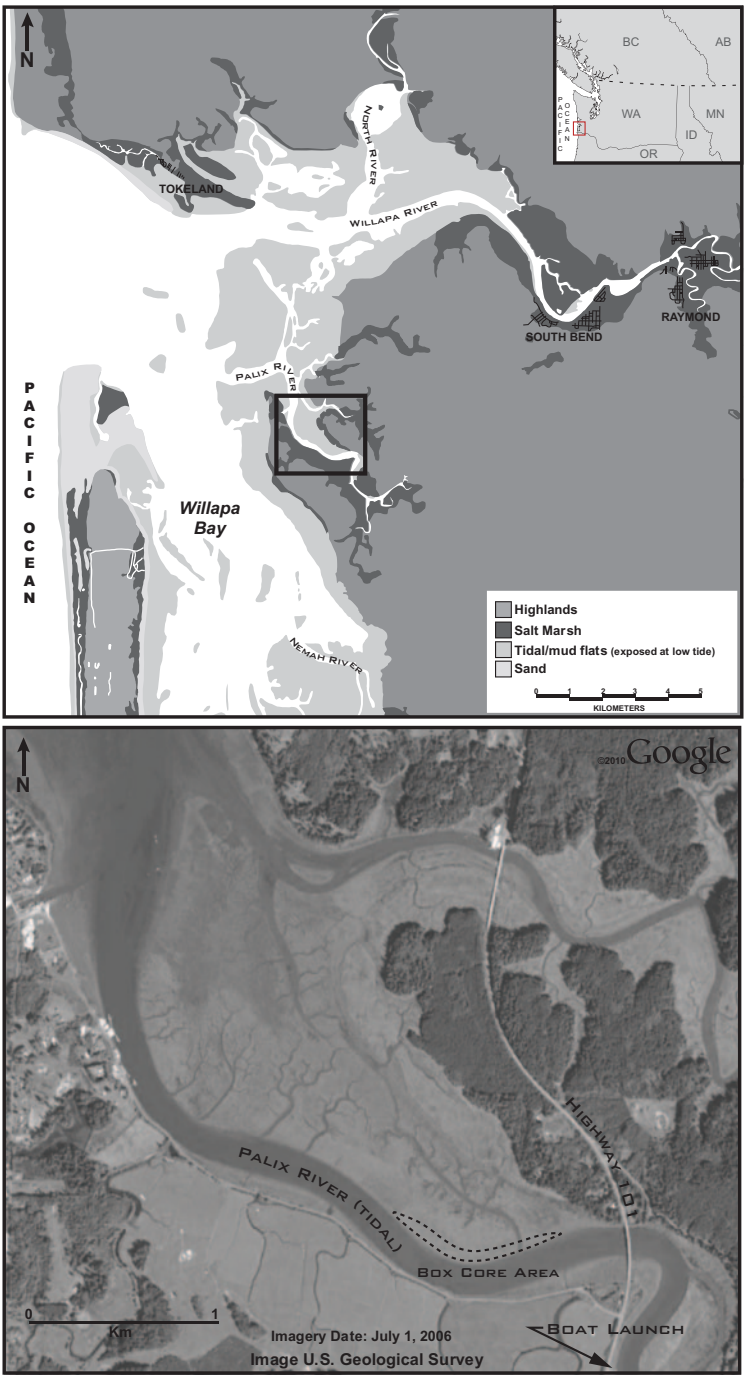

Fig. 9.1 Location map showing Willapa Bay (*top*) and the area where the box cores were retrieved (*dashed lines*). The footprint of the image in the bottom panel is shown with a heavy *black line* in the upper panel. The area is accessible with some scrambling from the HWY 101 bridge; however, safer access is to use a small watercraft from the public boat launch indicated at the *bottom right*. (Drafting courtesy of Jesse Schoengut)

Stations were chosen based on their position in the lower intertidal zone where open burrows were observed and in situ plants were absent. The stations were surveyed using a handheld Global Positioning System (GPS) with an accuracy of <10 m. Each station was sampled by collecting box core, and adjacent shovel samples were used to confirm the (macroscopic) animal content. Water was sampled from the adjacent channel.

The box cores measured 30 cm (vertical dimension) × 18 cm × 6 cm. X-rays were taken of the box cores using a Soyee portable X-ray system in plastic trays. The X-rays were collected 2 m from the source with a setting of 80 kVp/20 mA using exposure times between 1.5 and 1.7 s, depending on the mud content of the core. The X-rays provide images that reveal density contrasts. Greater densities are light colored (i.e., lower exposure of X-rays) and lesser densities are darker. In the case of the X-ray images in Fig. 9.2, void space is darkest, sand is darker than mud, and Fe minerals are lighter than the mud and sand phases (e.g., Fe-cemented burrow linings in Fig. 9.2c and d, yellow arrows). The distribution of burrows, sand, mud, and Fe cement was interpreted visually.

Mineral compositions of burrow lining and matrix were confirmed using a Rigaku Geigerflex Powder Diffractometer, equipped with a cobalt tube, graphite monochromator, and scintillation detector. The system had an online computer with analog and digital data processing capacity. Routine search/match was run on a separate computer using JADE 9.1 software and the International Centre for Diffraction Data and Inorganic Crystal Structure Database.

Water composition was determined using a Perkin Elmer Elan6000 quadrupole ICP-MS. For solution-mode analysis, a Perkin Elmer AS-91 automated sampling system was employed.

9.5 Results

Figure 9.2a shows a photograph of burrowed fresh sediment with ferric iron-stained burrow linings. The remaining images on Fig. 9.2 are X-ray plates that reveal horizontal bedding, bioturbation, iron-stained linings (see XRD results, below) (Fig. 9.2b–f), and amorphous "clouds" of Fe mineralization (Fig. 9.2e and f). Observations relating to burrow-associated Fe are separated from the description of the amorphous Fe clouds.

9.5.1 Bioturbation and Burrow Linings

Several tracemakers and their burrows are observed. U-shaped burrows (Fig. 9.2b) are made by the amphipod *Corophium volutator*. Dominantly vertical burrows with basal branches represent the domiciles of Nereid polychaetes (likely *Nereis virens*). Vertical burrows with a lower coil or loop represent the efforts of the enteropneust, *Saccoglossus kowalevskii* (Fig. 9.2c, leftmost burrow). Small-diameter burrows

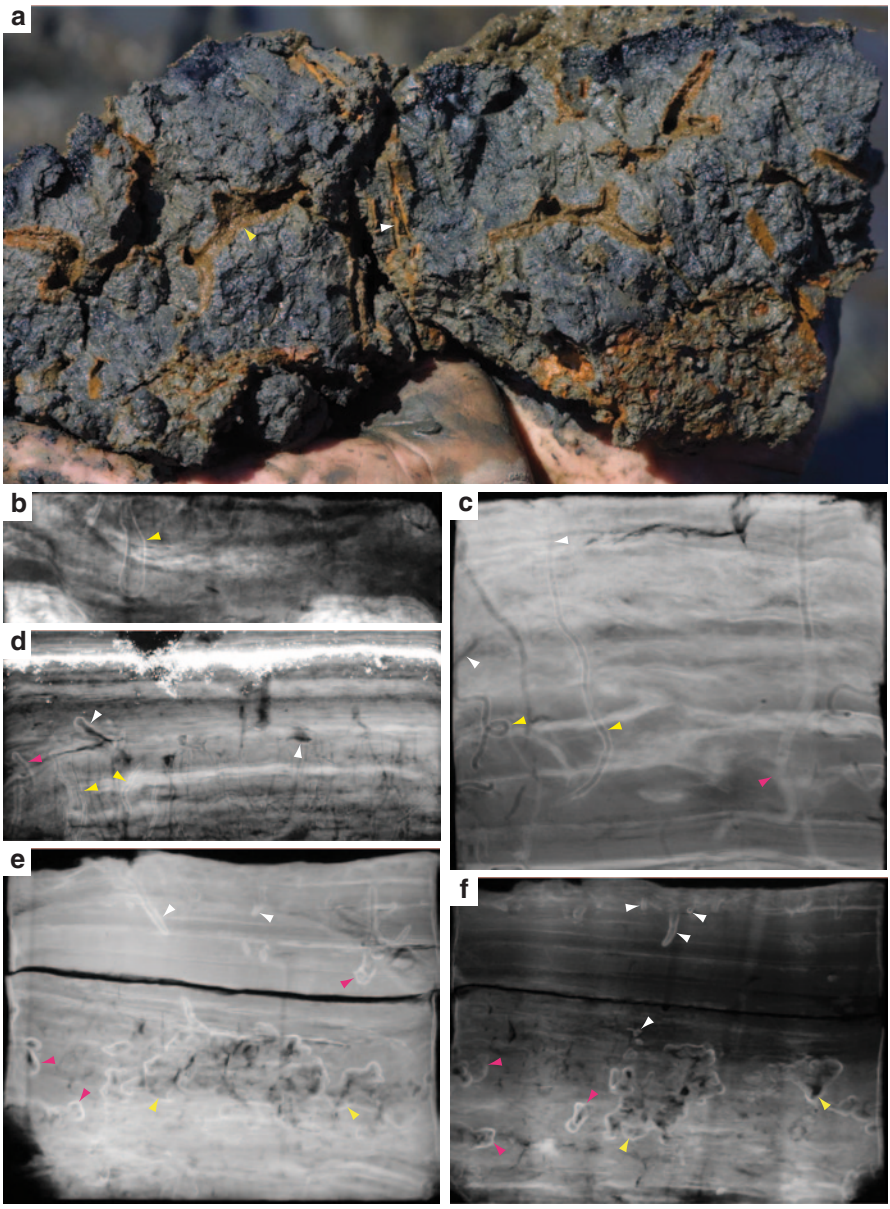

Fig. 9.2 Photograph and X-ray images of the Palix River intertidal sediments. The Fe-phase can be associated with color. Fe^{2+} is *bright orange* in color, with *deeper reds* associated with Fe^{3+}. The sulfide-bound Fe is *dark gray* to *black* (König et al. 1997). **a** Typical bioturbated intertidal sediment. The burrows are lined with amorphous Fe and/or maghemite. The darkest patches of sediment are sulfidic. This example is mixed sand and mud. Bedding is not visible, but X-rays confirm that the sediment is laminated and burrowed. Biogeochemical zones are evident as the *brown surface* and *burrow layer,* which grade into gray then black sediment. **b** *Arenicolites*-like burrow (made by *Corophium*) from the upper part of the box core. The *bright zone* is the location of

that shallowly penetrate are dominantly the work of spionid polychaetes (genus not determined). Small-diameter burrows that are observed several centimeters below the sediment–water interface are the burrows of *Heteromastus filiformis*.

Most of the open burrows show evidence of ferric iron mineralization on the burrow linings. In fresh sediment, this is observed as the orange-colored rims that contrast starkly against the dark, suboxic/anoxic sediment (Fig. 9.2a). Owing to the higher density of the ferric iron phases, they appear on all of the X-ray images as brightened linings. Burrow-associated Fe is typically <1 mm thick, is constrained to the burrow margin, and is prevalent in open burrows that have a connection to the sediment–water interface. The ferric iron lining is better developed below 2–10 cm depth, and commonly the upper part of the burrow has no observable Fe (Fig. 9.2c and d). Some burrows are partially infilled (e.g., Fig. 9.2c, pink arrow): In those examples, a ferric iron-enriched lining is not observed. Qualitatively, it appears that the locally coiled burrows of *Saccoglossus* have the best-developed ferric iron linings of the burrows observed (e.g., Fig. 9.2c) and some burrows, such as small U-shaped burrows near the sediment–water interface, have no discernible Fe-cement lining. Finally, Fig. 9.2d shows a level of burrows that have been buried by sedimentation. Although a few of these burrows still retain their ferric iron linings (yellow arrows), most of the burrows no longer possess them.

9.5.2 Reduced Iron Mineralization Zones

The other mode of iron mineralization occurs as halos around burrow fabrics. The halos are observed 2–10 mm away from, and surrounding, causative burrows (Fig. 9.2e and f, pink arrows). In extreme cases, the halos appear to coalesce into larger amorphous masses that are several centimeters across (Fig. 9.2e and f, yellow arrows). The halos are most common near burrows that have been infilled (Fig. 9.2d, pink arrow; Fig. 9.2e, white arrows) and near open burrows that have become isolated from the sediment–water interface (Fig. 9.2d, white arrows; Fig. 9.2e, yellow arrows; Fig. 9.2f, pink and yellow arrows).

Fig. 9.2 (continued) maghemite precipitation. **c** Burrows of the hemichordate *Saccoglossus* (*yellow arrows*) and *Nereis* (*pink arrow*). The *yellow arrows* also indicate areas of maghemite precipitation, whereas the *white arrows* indicate where no Fe precipitate is observable. The *pink arrow* shows an infilled part of the Nereid burrow that no longer possesses a Fe lining. **d** The burrows in the *lower part* of this image have been cut off from the sediment–water interface by previous erosion. Some burrows retain the maghemite lining (*yellow arrows*), but others do not. The *pink* and *white arrows* show areas where the Fe has diffused into the matrix and reprecipitated. The *bright zone* at the *top* of the image is a lead-shot layer emplaced for 612 months, before the sample was taken for the purpose of observing sedimentation rates. **e, f** *White arrows* indicate maghemite linings around unidentified burrows, the *pink arrows* indicate slightly remobilized Fe that is diffusing away from the burrow structures. The *yellow arrows* indicate clouds of pyrite that represent the remobilized and reprecipitated Fe. In both examples, the bedding is interpreted to represent seasonal banding resulting from mud- versus sand-dominated sedimentation in the winter and summer, respectively

9.5.3 XRD Mineralogy and Water Composition

X-ray diffraction (XRD) indicates that the burrow lining contains maghemite-C (an intermediate phase between magnetite and hematite) and typically forms via incomplete Fe(II) oxidation. The XRD signals from the analytes are weak, suggesting that some of the iron oxide is poorly crystalline. The matrix is dominated by quartz, albite and diopside, with minor pyrite. The pyrite is present as microscale framboids. XRD indicates that the pyrite is near-end-member and is neither Ni-bearing (bravoite) nor Co-bearing (cattierite). No maghemite is observed, suggesting that it is authigenically formed near burrow margins.

Inductively coupled plasma mass spectrometry (ICP-MS) analysis of the surface water collected during coring indicates a low Fe content, ~0.07 ppm. This is an order of magnitude higher than characteristic oceanic Fe concentrations (i.e., 0.0034 ppm; Turekian 1968).

9.6 Interpretation and Discussion

We propose that maghemite precipitates on the burrow margin where O_2 is present as a result of the animal's irrigation of the burrow. This process brings oxygenated water into the suboxic depths. Notably, O_2 does not diffuse far into the burrow lining. In a study of similar bioturbated media from the same area, Zorn et al. (2006) used an O_2 microsensor to show that O_2 diffusion into the suboxic sediment was generally limited to approximately 1 mm. The limited diffusion was ascribed to a low permeability of the sediment and a high organic content. Our observations of ferric iron present only as burrow linings, suggest a similar O_2 distribution.

Importantly, ferric iron precipitates are less common in the upper part of the burrows and are also not well developed, where the burrows have become isolated from the sediment–water interface or where the burrows are infilled. The local lack of a ferric iron precipitate near burrow apertures suggests that the Fe is primarily derived from the sediment pore water—this assertion is supported by the low concentrations of dissolved Fe measured in the depositional waters. The sediment is derived from weathering of basalt in the Willapa highlands and some Fe-rich phases, particularly clinopyroxene, are available as a source of Fe (Bynum 2007). The presence of Fe in the pore water may be explained by in situ dissolution of the detrital sediment. The Fe may also be delivered to the oceans by rivers, then bound as organometallic complexes and then deposited in association with clay minerals. Finally, Fe can also be provided through primary production. For example, many algae incorporate Fe as a trace element and some Fe may be added with the deposition of that biomass.

The Fe concentration of pore water is also a result of continuous Fe cycling in the sediment (i.e., enriched at the burrow margin, then reduced and mobilized back into the pore water). The subsequent dissolution of the ferric iron-rich linings, where

burrows are isolated from the surface or are in a state of infilling, likely occurred due to its remobilization via bacterial Fe(III) reduction. This process is driven by sediment-associated bacteria that derive their energy from the oxidation of buried organic compounds (including the burrow lining) and the concomitant reduction of ferric iron, which serves as the electron acceptor during metabolism. This process is common in marine anoxic sediments, after oxygen and Mn(IV) supplies are exhausted (see Konhauser 2007). The product of this reaction is dissolved Fe^{2+}, which then advects or diffuses away from the zone of reduction into the bulk matrix, where it is then either reoxidized (when O_2 is present) or it eventually precipitates as a ferrous-iron containing phase, such as pyrite (in saline waters) or siderite, $FeCO_3$ (in brackish waters). In our example, pyrite forms the halos and amorphous masses observed in the X-ray images.

The distribution of oxidized and reduced Fe phases in the sediment highlights the artifice of the general view of (bio)chemical zonation in marine sediments. In most of the models, the distributions of those chemical levels are portrayed as horizontal, planiform layers, also known as biogeochemical zones (seen in Fig. 9.2a as the brownish surface and burrow layer gradational to gray sediment and the black media) (König et al. 1997), that predict an orderly succession of microbial metabolites progressing from aerobic respiration, through various other metabolisms, and ultimately ending with methanogenesis at depth. Even models that account for bioturbation (Aller et al. 1998; Sandnes et al. 2000) (Fig. 9.3) have difficulties accounting for the chaotic distribution of burrows and variations in burrow distributions and depth over time. Rather, dynamic patterns of sedimentation and animal distribution for a sedimentary locale lead to the presence of burrows of variable depth, diameter, and shape, and different propensities to promote Fe mineralization. Much larger reactive surface areas contribute to greater quantities of Fe accumulating in the sediment. Fe may be reduced and precipitated as pyrite, only to be exposed to later bioturbation and thereby reoxidized (Fig. 9.3). The distributions of Fe minerals do not stabilize until the sediment passes beyond the reach of burrowing animals.

An aspect of the X-ray data is that the formation of inchoate pyrite nodules is visualized. In the provided examples, the Fe^{2+} is first concentrated within biogenic sedimentary structures, it becomes oxidized to maghemite, then subsequently reduced and redistributed as pyrite halos. Although it is not certain how long this process takes, some temporal constraints can be made from the dataset. A general observation at this location, having initiated research there in 1996, is that winter sedimentation is dominated by mud and summer sedimentation is prone to deposition of very fine sand laminae. As such, each centimeter-scale mud-sand couplet can be interpreted as a varve. Figure 9.2d, for example shows that the lower burrows are truncated approximately 3 years prior to the box-core sampling: Therein, many of the burrows have only vague ferric iron-rich linings and locally thin haloes have begun to form. The coalescent pyrite masses observed in Fig. 9.2e and f show six “annual” layers above the burrowed zone and we infer those to have been buried for 6 years before sampling: Incipient nodule formation seems to occur quite rapidly.

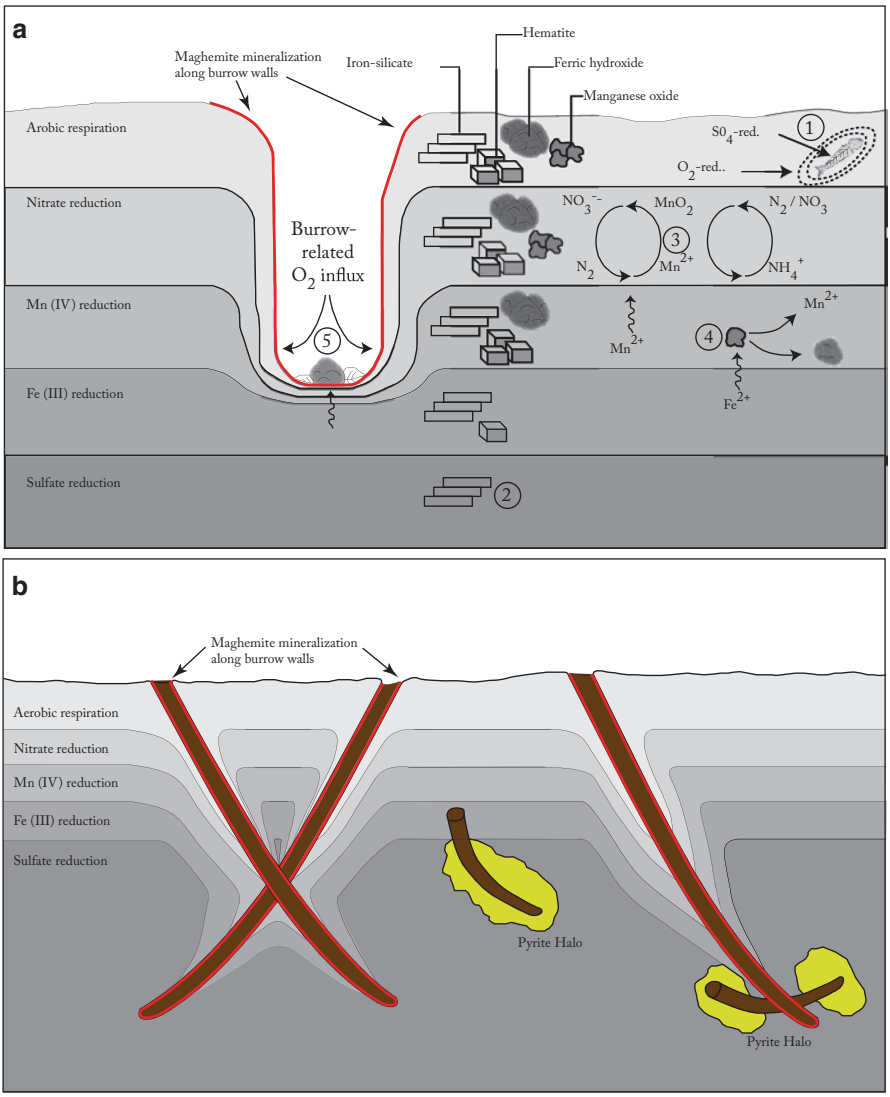

Fig. 9.3 Schematic models of geochemical levels in marine sedimentary environments. **a** Most conceptual models denote planiform chemoclines that deflect around simple burrow morphologies and may locally extend certain bacterial lifestyles deeper into the sediment (modified from Konhauser 2007). **b** Burrows generally are more complicated than the simple conceptualization and, as such, the distributions of geochemical processes are spatially complex. Also, the reactive surface area is larger. Abandoned burrows are compositionally different than the surrounding sediment and add compositional heterogeneity within geochemical zones

There are several examples of nodules that have a ferric iron core with later-stage pyrite encompassing them. These nodules are common in marginal marine strata (personal observation) and they occur in three ways: around fossil roots, in association with burrows, and as crudely spherical nodules with massive appearing

goethite at their cores. Such nodules are normally taken to indicate compositionally evolving pore water (Al-Agha et al. 1995). Another explanation is that, similar to this modern example, the minerals are essentially contemporaneous and are more closely related to the nature of Fe cementation in association with biogenic sedimentary structures.

9.7 Conclusions

Through the efficacy of X-rays for the observance of Fe mineralization in intertidal sediments, it is possible to model the distribution and cycling of Fe minerals in those deposits. In general, the source of Fe is the sediment itself, which, in this case, was derived from weathered basalts. The Fe then precipitates as maghemite on burrow linings. Following burrow abandonment or burial, the ferric iron is reduced and precipitates as pyrite haloes around the burrow fabrics. Based on the knowledge of the sedimentation rates and analysis of the sedimentary fabric, it seems likely that inchoate nodules form over the period of a few years. There are several limitations to this study: (1) Independent assessment of sedimentation rates would help interpret the temporal aspects of the Fe mineralization; (2) analysis of the fluvial sediment in the river proper might reveal the specific source of Fe; and (3) analysis of Fe-rich burrows versus burrow types that are less prone to Fe mineralization would be useful. These issues should be addressed in future research.

Acknowledgments This work was funded by NSERC Discovery Grants to MKG, JPZ, and KOK.

References

Al-Agha MR, Burley SD, Curtis CD, Esson J (1995) Complex cementation textures and authigenic mineral assemblages in recent concretions from the Lincolnshire Wash (East coast, UK) driven by Fe(0) to Fe(II) oxidation. J Geol Soc Lond 152:157–171

Aller RC (1980) Quantifying solute distributions in the bioturbated zone of marine sediments by defining an average microenvironment. Geochim Cosmochim Acta 44(12):1955–1966

Aller RC, Hall POJ, Rude PD, Aller JY (1998) Biogeochemical heterogeneity and suboxic diagenesis in hemipelagic sediments of the Panama Basin. Deep-Sea Res Part I 45(1):133–165

Bynum GL (2007) Heavy-mineral provenance in an estuarine environment, Willapa Bay, Washington, USA: palaeogeographic implications and estuarine evolution. In: Mange MA (ed) Heavy minerals in use. Developments in sedimentology, vol 58. Elsevier, Amsterdam, pp 587–605

Carpenter SJ, Erickson JM, Lohmann KC, Owen MR (1988) Diagenesis of fossiliferous concretions from the Upper Cretaceous Fox Hills Formation, North Dakota. J Sediment Petrol 58(4):706–723

Clifton HE (1983) Discrimination between subtidal and intertidal facies in Pleistocene deposits, Willapa Bay, Washington. J Sediment Petrol 53(2):353–369

Corlett HJ, Jones B (2012) Petrographic and geochemical contrasts between calcite- and dolomite-filled burrows in the Middle Devonian Lonely Bay Formation, Northwest Territories, Canada: implications for dolomite formation in Paleozoic burrows. J Sediment Res 82:648–663

Ferreira TO, Otero XL, Vidal-Torrado P, Macias F (2007) Effects of bioturbation by root and crab activity on iron and sulfur biogeochemistry in mangrove substrate. Geoderma 142(1–2):36–46

Gingras MK, Pemberton SG, Saunders T, Clifton HE (1999) The ichnology of modern and Pleistocene brackish-water deposits at Willapa Bay, Washington: variability in estuarine settings. Palaios 14(4):352–374

Gingras MK, Pemberton SG, Muehlenbachs K, Machel H (2004) Conceptual models for burrow-related, selective dolomitization with textural and isotopic evidence from the Tyndall Stone, Canada. Geobiol 2(1):21–30

Konhauser KO (2007) Introduction to geomicrobiology. Blackwell Publishing, Oxford

Konhauser KO, Gingras MK (2007) Linking geomicrobiology with ichnology in marine sediments. Palaios 22(4):339–342

König I, Drodt M, Suess E, Trautwein AX (1997) Iron reduction through the tan-green color transition in deep-sea sediments. Geochim Cosmochim Acta 61:1679–1683

Löwemark L, Schäfer P (2003) Ethological implications from a detailed X-ray radiograph and C-study of the modern deep-sea *Zoophycos*. Palaeogeogr Palaeoecol 192(14):101–121

Over DJ (1990) Trace metals in burrow walls and sediments, Georgia Bight, USA. Ichnos 1(1):31–41

Rameil N (2008) Early diagenetic dolomitization and dedolomitization of Late Jurassic and earliest Cretaceous platform carbonates: a case study from the Jura Mountains (NW Switzerland, E France). Sediment Geol 212:70–85

Rodriguez-Tovar F (2005) Fe-oxide spherules infilling *Thalassinoides* burrows at the Cretaceous-Paleogene (K-P) boundary: evidence of a near-contemporaneous macrobenthic colonization during the K-P event. Geol 33(7):585–588

Sandnes J, Forbes T, Hansen R, Sandnes B, Rygg B (2000) Bioturbation and irrigation in natural sediments, described by animal-community parameters. Mar Ecol Prog Ser 197:169–179

Turekian KK (1968) Oceans. Prentice-Hall, New Jersey

Virtasalo JJ, Whitehouse MJ, Kotilainen AT (2012) Iron isotope heterogeneity in pyrite fillings of Holocene worm burrows. Geol 41(1):39–42

Wetzel A (2008) Recent bioturbation in the deep South China Sea: a uniformitarian ichnologic approach. Palaios 23(9):601–615

Zorn ME, Lalonde SV, Gingras MK, Pemberton SG, Konhauser KO (2006) Microscale oxygen distribution in various invertebrate burrow walls. Geobiol 4:137–145